Articles

The Presence of a Hydrogen Bond between Asparagine 485 and the π System of FAD Modulates the Redox Potential in the Reaction Catalyzed by Cholesterol Oxidase[†,‡]

Ye Yin,[§,||] Nicole S. Sampson,*[,||] Alice Vrielink,*[,⊥,#] and Paula I. Lario[§,⊥,#]

Department of Molecular, Cellular, and Developmental Biology, Sinsheimer Laboratory, University of California, Santa Cruz, Santa Cruz, California 95064, Biochemistry Department, McGill University, Montréal, QC, H3G-1Y6 Canada, and Department of Chemistry, State University of New York at Stony Brook, Stony Brook, New York 11794-3400

Received April 24, 2001; Revised Manuscript Received August 17, 2001

ABSTRACT: Cholesterol oxidase catalyzes the oxidation and isomerization of cholesterol to cholest-4-en-3-one. An asparagine residue (Asn485) at the active site is believed to play an important role in catalysis. To test the precise role of Asn485, we mutated it to a leucine and carried out kinetic and crystallographic studies. Steady-state kinetic analysis revealed a 1300-fold decrease in the oxidation k_{cat}/K_m for the mutant enzyme whereas the k_{cat}/K_m for isomerization is only 60-fold slower. The primary kinetic isotope effect in the mutant-catalyzed reaction indicates that 3α-H transfer remains the rate-determining step. Measurement of the reduction potentials for the wild-type and N485L enzymes reveals a 76 mV decrease in the reduction potential of the FAD for the mutant enzyme relative to wild type. The crystal structure of the mutant, determined to 1.5 Å resolution, reveals a repositioning of the side chain of Met122 near Leu485 to form a hydrophobic pocket. Furthermore, the movement of Met122 facilitates the binding of an additional water molecule, possibly mimicking the position of the equatorial hydroxyl group of the steroid substrate. The wild-type enzyme shows a novel N−H···π interaction between the side chain of Asn485 and the pyrimidine ring of the cofactor. The loss of this interaction in the N485L mutant destabilizes the reduced flavin and accounts for the decreased reduction potential and rate of oxidation. Thus, the observed structural rearrangement of residues at the active site, as well as the kinetic data and thermodynamic data for the mutant, suggests that Asn485 is important for creating an electrostatic potential around the FAD cofactor enhancing the oxidation reaction.

Cholesterol oxidase (EC 1.1.3.6) is a flavoenzyme isolated from a variety of microorganisms. It is able to catalyze two reactions in one active site: oxidation of the 3β-hydroxyl of cholesterol and subsequent 1,3-allylic isomerization of the oxidation product (Scheme 1). It is used to clinically determine serum cholesterol levels in the diagnosis of arteriosclerosis and other lipid disorders. The active enzyme is a potent larvicide and is being developed for commercial applications in agriculture as a pest control agent (*3*−*5*). Moreover, cholesterol oxidase is utilized to study membrane structures, especially the localization of cholesterol. With the precise elucidation of the atomic-level mechanism of cholesterol oxidase catalysis and binding of steroid, both fundamental studies and practical uses will be greatly advanced.

Cholesterol oxidases from *Streptomyces sp. SA-COO* and *B. sterolicum* are monomeric (55 kDa) proteins (60% identical in amino acid sequence) containing one FAD[1] per active site (*6*). There is little (<10%) primary sequence similarity between cholesterol oxidase and other members of the glucose−methanol−choline oxidoreductase (GMC) family (*7*, *8*). However, comparison with the tertiary structures of GMC oxidoreductase enzymes shows that their overall architecture is conserved. His447, Asn485,[2] Glu361, and Wat541 are all highly conserved among cholesterol

[†] This work is supported by NIH Grants HL-53306 (N.S.S.) and GM63262 (A.V.), by MRC Grant MT-13341 (A.V.), and by a McGill Faculty of Medicine Internal Studentship (P.I.L.). The Spex fluorimeter was purchased with a grant from the NSF (CHE 9709164).

[‡] The coordinates have been deposited with the Brookhaven Protein Data Bank (PDB code 1IJH).

* To whom correspondence should be addressed. N.S.S.: telephone (631) 632-7952, fax (631) 632-5731, e-mail nicole.sampson@sunysb.edu. A.V.: telephone (831) 459-3929, fax (831) 459-3139, e-mail vrielink@biology.ucsc.edu.

[§] These authors contributed equally to this work.

[||] State University of New York at Stony Brook.

[⊥] University of California, Santa Cruz.

[#] McGill University.

[1] Abbreviations: chox, cholesterol oxidase; choA, *Streptomyces* cholesterol oxidase; LB, Luria broth; IPTG, isopropyl β-D-thiogalactoside; SDS−PAGE, sodium dodecyl sulfate−polyacrylamide gel electrophoresis; DEAE, diethylaminoethyl; TLC, thin-layer chromatography; HRP, horseradish peroxidase; 2 × YT, 2 × yeast−tryptone broth; BSA, bovine serum albumin; GMC, glucose−methanol−choline; FAD, flavin adenine dinucleotide; OPA, opal stop codon.

[2] This numbering refers to the X-ray crystal structure system for numbering amino acid residues (*1*). Asn485 is encoded by codon 522 in the *Streptomyces* gene (*2*).

10.1021/bi010843i CCC: $20.00
Published on Web 10/26/2001

Scheme 1

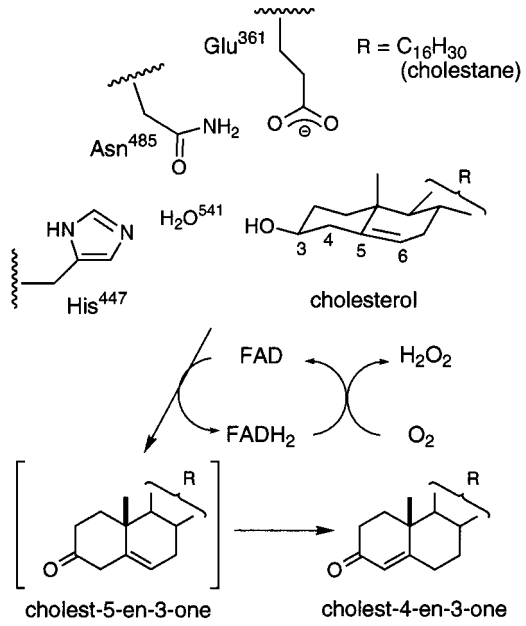

oxidases where the FAD cofactor is noncovalently bound to the enzyme. We have proposed that a hydrogen-bonding network between these residues helps to position the substrate relative to the FAD cofactor and coordinates general base and electrophilic catalysis for oxidation (*6*, *9*). The X-ray crystal structure suggested that His447 could coordinate general base catalysis of oxidation via Wat541 (*6*, *10*). We showed that His447 is important for oxidation, but is not essential. Replacement of the imidazole with a glutamine amide resulted in a 100-fold reduction in the overall rate of oxidation, and hydride transfer was no longer rate-determining.[3] This suggested that additional residues might contribute to catalysis of oxidation. In this work, we investigated the role of Asn485 in the reaction catalyzed by cholesterol oxidase by a combination of site-directed mutagenesis, kinetics, and X-ray crystallography. We found that this residue is crucial for defining the electrostatic environment around the FAD that determines its reduction potential.

EXPERIMENTAL PROCEDURES

Materials. Cholest-5-en-3-one, 4-aminoantipyrine, and Triton X-100 were from Aldrich Fine Chemical Co. (Milwaukee, WI). Cholesterol and horseradish peroxidase were purchased from Sigma Chemical Co. (St. Louis, MO). The plasmid for heterologous expression of *Streptomyces sp. SA-COO* cholesterol oxidase, pCO202, has been described previously (*11*), and is a derivative of pCO117, a generous gift from Y. Murooka (*12*). Restriction endonucleases, T4 DNA ligase, calf intestinal alkaline phosphatase, and T4 kinase were purchased from New England Biolabs (Beverly, MA). Oligonucleotides were purchased from IDT, Inc. (Coralville, IA). All other chemicals and solvents, of reagent or HPLC grade, were supplied by Fisher Scientific (Pittsburgh, PA). Water for assays and chromatography was distilled, followed by passage through a Barnstead NANOpure filtration system to give a resistivity better than 18 MΩ.

General Methods. CD spectra were acquired on an Aviv model 62A circular dichroism spectrophotometer. A Shimadzu UV2101 PC spectrophotometer was used for assays and acquisition of UV spectra. Fluorescence measurements were taken on a Spex Fluorolog 3-11 spectrofluorometer. Restriction digests and ligations were performed according to procedures described in Sambrook et al. (*13*). The ABI PRISM BigDye Terminator Cycle Sequencing technique was applied to all mutated regions following the manufacturer's protocol (Perkin-Elmer, Foster City, CA), and the plasmids were purified with the Wizard Plus DNA Purification System (Promega, Madison, WI) with water elution. The buffers used were the following: A: 50 mM sodium phosphate, pH 7.0; B: buffer A + 0.025% Triton X-100 (w/v); C: buffer B + 0.020% BSA (w/v); D: buffer A + 1.0 M $(NH_4)_2SO_4$; E: 100 mM citrate−phosphate, pH 5.10, 0.025% Triton X-100 (w/v); F: 100 mM sodium phosphate, pH 5.90, 0.025% Triton X-100 (w/v); G: 100 mM sodium phosphate, pH 6.96, 0.025% Triton X-100; H: 100 mM sodium phosphate, pH 8.18, 0.025% Triton X-100; I: 100 mM glycine−NaOH, pH 9.06, 0.025% Triton X-100; J: 100 mM glycine−NaOH, pH 9.98, 0.025% Triton X-100.

Construction of N485L ChoA Mutant Expression Plasmid, pCO237. In addition to introducing the N485L mutation, the extraneous *Streptomyces* DNA between the OPA and the *Hin*dIII site in pCO200 (*11*) was removed by PCR using two primers. Primer 1 was a 67-base oligonucelotide that corresponded to the sequence of the coding strand (5′-ggCTggggCCCCAACggTAACATCATgACCgCCCgggCCAACCACAtgKBTAACCCCACCggCgCCC-3′). This primer was upstream of a *Stu*I site that was used for subcloning the PCR fragment. Primer 2 was a 99-base oligonucleotide that possessed the actual mutation N485L, introduced a *Hin*dIII site after the TAA stop codon, and corresponded to the anticoding strand (5′-gCTCACAAgCTTACgACgCCgTgACgTCCTgCTTgATgAtgCgCTCgACgTTCCgCTCggCCAgCgCCgTgATggTCACgAACgggAggACgCCgACgg-3′). Using *Xho*I-restricted pCO202 (*9*) as a template, 31 cycles of PCR were performed with Pfu polymerase at an annealing temperature of 75 °C. The 500 bp PCR fragment was digested with *Stu*I and *Hin*dIII, purified, and subcloned into pCO200 (*9*) that had been similarly digested to yield the mutant expression plasmid pCO237.

Purification of Wild-Type Cholesterol Oxidase. Cell paste of *E. coli* BL21(DE3)plysS(pCO117) (*11*) was obtained from 1 L of 2 × YT−ampicillin (200 μg/mL) medium grown at 28 °C for 8 h after addition of IPTG (100 μg/mL) at A_{600} = 0.8 by centrifugation at 4000*g* for 30 min. The pellet was resuspended in 20 mL of buffer A and lysed by French press at 18 000 psi. All subsequent steps for wild-type cholesterol oxidase were conducted at 4 °C. Cell debris was removed by centrifugation at 135000*g* for 60 min. The supernatant was precipitated by 1.0 M $(NH_4)_2SO_4$, and the pellet was discarded. $(NH_4)_2SO_4$ was added to the supernatant to a final concentration of 2 M. The pellet was obtained by centrifuga-

[3] The oxidation reaction catalyzed by chox utilizes a FAD cofactor, and thus may proceed as a hydride transfer, or it may proceed as two 1 e^- transfer steps, one of which is a hydrogen atom transfer. Both mechanisms would proceed more efficiently with general base catalysis, and from a structural viewpoint, both are feasible. For the sake of simplicity, we will discuss our experiments in reference to the hydride mechanism, although the arguments presented apply equally well to a two-step mechanism, i.e., hydrogen atom transfer followed by fast e^- transfer.

tion at 4000*g*. This pellet was resuspended in buffer A (5 mL) and desalted using dialysis (nMWCO 6000−8000) against buffer A. The dialysate was loaded onto a column of DEAE-cellulose (30 mm × 25 cm, DE-52, Whatman) preequilibrated with buffer A. Fractions were collected by elution with buffer A (100 mL). Typically, 15 mL fractions were collected; however, fractions that appeared yellow in color were limited to 7.5 mL. Fractions containing cholesterol oxidase (as determined by SDS−PAGE) were combined and concentrated by $(NH_4)_2SO_4$ precipitation (3.0 M). The pellet was redissolved in buffer A to give a final concentration between 10 and 20 mg/mL protein, and $(NH_4)_2SO_4$ was slowly added until the solution turned slightly turbid (typically, 2.5 M). The precipitate formed was pelleted by centrifugation, and the clarified supernatant was transferred to a fresh container where it was allowed to crystallize over 2 days at 4 °C. The microcrystalline protein was collected by centrifugation, dissolved in buffer A, and ultrafiltered (YM30 membrane, Amicon, Inc., Danvers, MA) into buffer A. The protein was further purified on a butyl-Sepharose column (30 mL butyl-Sepharose-4 Fast Flow, XK 16/40, Pharmacia Biotech, Upsala, Sweden) preequilibrated with buffer D. The protein was eluted by running a linear gradient from 100% buffer D to 100% buffer A (270 mL). Fractions (4.5 mL) were collected, and the elution profile was monitored at A_{280}. Fractions were assayed for content and purity by SDS−PAGE. Fractions containing pure cholesterol oxidase (>98%) were combined and ultrafiltered (YM30 membrane) into buffer A. Typically 30−40 mg of pure cholesterol oxidase was obtained per liter of culture.

Purification of N485L Cholesterol Oxidase. The mutant N485L cholesterol oxidase was prepared as described above for wild type. The yield of N485L was 75 mg/L. Protein concentrations were determined by UV absorbance using $\epsilon_{280} = 81\,924\ M^{-1}\ cm^{-1}$ [calculated from the molar extinction coefficients of tryptophan and tyrosine (*14*)].

UV, Fluorescence, and CD Spectra. Solutions of cholesterol oxidases were prepared in buffer A. A baseline spectrum of buffer A was subtracted from the sample spectrum. The concentrations of wild type and N485L used were 19 and 21 μM, respectively. CD spectra were recorded in the near UV from 300 to 255 nm, and in the far UV from 250 to 185 nm. The UV/vis spectra of the semiquinone and reduced flavin enzyme species were obtained during the anaerobic titration (vide infra), and the spectra were deconvoluted by subtracting the spectra of the other species present from the observed spectrum. The concentration of cholesterol oxidases used for fluorescence spectra was 2 μM.

Steady-State Enzyme Kinetics. Stock solutions of cholesterol and 3α-[^{2}H]-cholesterol were prepared by dissolving the appropriate sterol in propan-2-ol. The concentration of each solution was determined using cholesterol oxidase and standard assay condition 1 (vide infra). Stock solutions of cholest-5-en-3-one were prepared and stored in the dark in foil-wrapped containers because the cholest-5-en-3-one decomposes via autoxidation in solution; TLC (15:85, EtOAc:hexane ratio) was employed to assay the solutions for purity prior to use each day.

HRP (1000 units/mL), phenol (113 mM), and 4-aminoantipyrine (440 mM) stock solutions were prepared in buffer B. Dilute enzyme stock solutions were prepared in buffer C. The concentration of each enzyme used in assays with cholesterol was as follows: wild type, 0.55 nM; N485L, 86 nM. The concentration of each enzyme used in assays with cholest-5-en-3-one was as follows: wild type, 0.44 nM; N485L, 12 nM. Initial velocities were measured in one of three ways. (1) The formation of conjugated enone was followed as a function of time at 240 nm ($\epsilon_{240} = 12\,100\ M^{-1}\ cm^{-1}$) (*15*). (2) The activity also was determined using a horseradish peroxidase coupled assay to quantitate the rate of formation of H_2O_2. The formation of quinoneimine at 510 nm was followed as a function of time. The standard assay conditions were the same as the UV A_{240} assay with addition of 1.13 mM phenol, 0.87mM 4-aminoantipyrine, and 10 units of horseradish peroxidase. (3) The reaction was followed by excitation at 325 nm and monitoring the fluorescence emission at 415 nm (slits = 1.5 nm) using an HRP-coupled assay to quantitate the rate of formation of H_2O_2. The standard assay conditions were the same as the UV A_{240} assay with the addition of 1.0 mM *p*-hydroxyphenylacetic acid and 10 units of horseradish peroxidase. Independent sets of data were fit simultaneously to the hyperbolic form of the Michaelis−Menten equation using Grafit (Erithacus, London, U.K.). Primary isotope effects were determined in a similar fashion, fitting all the possibilities and selecting the best fit (^DV, $^DV/K$, or ^DV and $^DV/K$). pH profiles were determined using buffers E−J that had equal ionic strengths.

Determination of Reduction Potentials. The redox potentials of wild-type and mutant cholesterol oxidases were determined at pH 7.0, at 15 °C, using the dye-equilibration method and xanthine/xanthine oxidase reduction system described by Massey (*16*). Enzyme (10−15 μM) was placed in an anaerobic cuvette in buffer A, together with 0.2−0.3 mM xanthine and 1−10 μM concentrations of safranin T that has an E_m of −276 mV. To ensure rapid equilibration of reducing equivalents, 5 μM benzyl viologen was added to the enzyme solution. The closed cuvette was made anaerobic by repeated cycles of evacuation and flushing with argon. After anaerobiosis had been established, the spectrum of the enzyme solution was recorded. The reaction was initiated by adding xanthine oxidase from the sidearm, and absorbance spectra were recorded (300−800 nm). The absorbance spectra were collected until the contribution of the benzyl viologen radical became apparent.

The concentrations of the oxidized, semiquinone, and reduced forms of cholesterol oxidases, and of the oxidized and reduced forms of the reference dye, were determined from the absorbance values at various wavelengths (using an isosbestic point for the oxidized and semiquinone enzyme forms of 524.5 and 525.0 nm for wild type and N485L, respectively). The redox potential, E_h, for the system at equilibrium was calculated using the standard Nernst equation:

$$E_h = E_m + (2.3RT/nF)\ \log\ ([\text{oxidized form}]/[\text{reduced form}]) \quad (1)$$

The data were plotted as described previously (*16*). Briefly, the oxidation/reduction potential for the couple EFl_{ox}/EFl_{seq} (E_1) was determined by plotting the ratio of the concentrations of the oxidized and semiquinone forms of cholesterol oxidase, and the potential for the couple EFl_{seq}/EFl_{red} (E_2) was determined by plotting the ratio of the concentrations of the semiquinone and reduced forms of the enzyme. The

separation between the two single-electron transfers was estimated from the maximal percentage of the semiquinone form of the enzyme reached during a reduction experiment in the absence of the reference dye (*17*):

$$\Delta E_m = 59\ \text{mV} \times \log K \quad (2)$$

$$K = [\text{EFl}_{seq}]^2/[\text{EFl}_{red}][\text{EFl}_{ox}] \quad (3)$$

Semiquinone formation was graphically determined by plotting the changes in absorbance at the maximum wavelength for this form (372.5 and 376.5 nm for wild-type and N485L cholesterol oxidase, respectively) and for the oxidized enzyme (390.5 and 394.0 nm for wild-type and N485L cholesterol oxidase, respectively). The ΔE_m between the reference dye and cholesterol oxidase was determined from the value of log (oxidized/reduced) for the enzyme at the point where the log (oxidized/reduced) for the reference dye is zero.

Crystallographic Structure Determination. Crystals of the N485L mutant of cholesterol oxidase were obtained as described previously (*6*). X-ray diffraction data were collected at 115 K in order to minimize crystal decay. The crystals were transferred briefly to a cryoprotectant solution containing 20% glycerol in the crystal mother liquor. A single crystal was mounted in a cryoloop (Hampton Research, Laguna Hills, CA) and placed in a cold nitrogen stream at 115 K. The data were collected on a MAR image plate detector with a double focusing mirror system (Supper Ltd.) mounted on a Rigaku RU-200 rotating anode X-ray generator (CuKα radiation). A data set to 1.5 Å resolution was collected using a single crystal of dimensions 0.1 × 0.1 × 0.08 mm. The completeness of the data collected was 93% with a redundancy of 4 and a merging *R*-factor of 0.045. The X-ray images were processed, merged, and scaled with the HKL suite of software (*18, 19*). The mutant structure was solved by difference Fourier techniques using the native structure (PDB code 1b4v) which had been modified such that all active site water molecules and water molecules located on the surface of the structure were removed. In addition, the proposed catalytic residues, H447, N485, and E361, were mutated to alanines. Refinement was carried out using SHELX-97 (*20*) and SIGMAA-weighted maps calculated with coefficients $2F_o - F_c$ and $F_o - F_c$. The free *R*-factor was monitored during the course of the refinement using a subset of 10% of the data randomly chosen from the total diffraction data. The entire structure was rebuilt, and the side chains for H447 and E361 as well as the leucine mutation at position 485 were included in the model. Water molecules were included where difference electron density above 3σ was observed and where hydrogen bond contacts were made to other polar atoms. Multiple conformations were included for a loop region of the structure (256−260) as well as a 10 amino acid side chain. In addition, the side chains of nine surface residues were modeled with partial occupancy. The final refinement statistics are given in Table 1. The coordinates have been deposited in the Protein Data Bank (*21*).

Table 1: Crystallographic Refinement Statistics

resolution range (Å)	25−1.5
total reflections used in refinement	57331
R-factor	0.163
free *R*-factor	0.213 (6632 reflections)
rmsd bond lengths (Å)	0.009
rmsd bond angle distances (Å)	0.024
no. of non-hydrogen atoms	
protein	3901
FAD	53
water	611
average *B*-factors (Å^2)	
overall	16.8
protein atoms	15.6
FAD atoms	10.3
water molecules	25.5

RESULTS

Physical Characterization. The N485L cholesterol oxidase was heterologously expressed in *E. coli.* The purity was confirmed by SDS−PAGE analysis, UV/vis, and CD spectroscopy. The UV spectrum of the bound FAD cofactor for the purified N485L cholesterol oxidase has red-shifted λ_{max}'s at 394 and 472 nm compared to wild type at 390.5 and 468 nm (Figure 1). The fluorescence emision maxima for wild-type and N485L are the same: 338 nm (280 nm, excitation), 526 nm (450 nm, excitation). The CD spectra (far and near UV) confirm that the N485L mutant is folded identically to wild type.

Steady-State Kinetics. The catalytic capability of the N485L mutant is summarized in Table 2 along with previously obtained data on the H447Q mutant. The Michaelis−Menten parameters of the active mutants using both cholesterol and cholest-5-en-3-one as substrates are reported. In the wild-type catalyzed reaction using cholesterol as a substrate, the A_{240}-based assay that follows the rate of product cholest-4-en-3-one formation and the H_2O_2-based assay that follows the rate of intermediate product H_2O_2 formation measure the same steady-state rates. The rate constants for both assays of the N485L mutant are also the same. This means that N485L catalyzes oxidation and isomerization; i.e., it converts cholesterol to cholest-4-en-3-one. However, the k_{cat}/K_m is 1300-fold reduced compared to wild type.

The mutant isomerization activity using cholest-5-en-3-one as a substrate was compared with wild-type cholesterol oxidase by monitoring the rate of cholest-4-en-3-one appearance at 240 nm. The ability of wild-type enzyme to catalyze the isomerization of the cholest-5-en-3-one is as efficient as its ability to oxidize and isomerize cholesterol. The isomerization k_{cat}/K_m of N485L is 60-fold slower than wild type.

Primary Isotope Effects. The same substrate primary kinetic isotope effects were observed for wild-type cholesterol oxidase and the N485L mutant using 3α-[^{2}H]-cholesterol. The isotope effects are 2.2 ± 0.1 on both k_{cat} and k_{cat}/K_m.

pH−Rate Profile. The pH dependence of the cholesterol oxidation reaction was measured by following the appearance of cholest-4-en-3-one, the product of oxidation and isomerization. For wild-type cholesterol oxidase, the value of k_{cat} decreased 2000-fold with increasing pH with an apparent pK_a of 8.3 ± 0.1; the K_m was independent of pH. The loss of activity is reversible. In contrast, an increase in pH for the N485L mutant resulted in a 6-fold increase in the k_{cat}. The pK_a(app) for k_{cat} is 9.5 ± 0.3; again, K_m did not change with pH. The isomerization activity of N485L or wild type did not change with increasing pH.

Table 2: Michaelis-Menten Rate Constants for Wild-Type and Mutant Cholesterol Oxidases

	turnover (oxidation and isomerization) cholesterol[a]			isomerization cholest-5-en-3-one[b]		
	k_{cat} (s^{-1})	K_m (μM)	$(k_{cat}/K_m)_{mut}/(k_{cat}/K_m)_{wt}$	k_{cat} (s^{-1})	K_m (μM)	$(k_{cat}/K_m)_{mut}/(k_{cat}/K_m)_{wt}$
wild type	44 ± 2	3.0 ± 0.4		64 ± 3	6.2 ± 0.7	
H447Q[c]	0.32 ± 0.01	3.0 ± 0.3	0.0036	81 ± 4	7.1 ± 0.8	1.1
N485L	0.046 ± 0.004	4.2 ± 0.1	0.00075	3.2 ± 0.3	18 ± 0.6	0.017

[a] Measured by H_2O_2 formation with HRP coupling. [b] Measured by cholest-4-en-3-one formation at 240 nm. [c] As reported in (*9*).

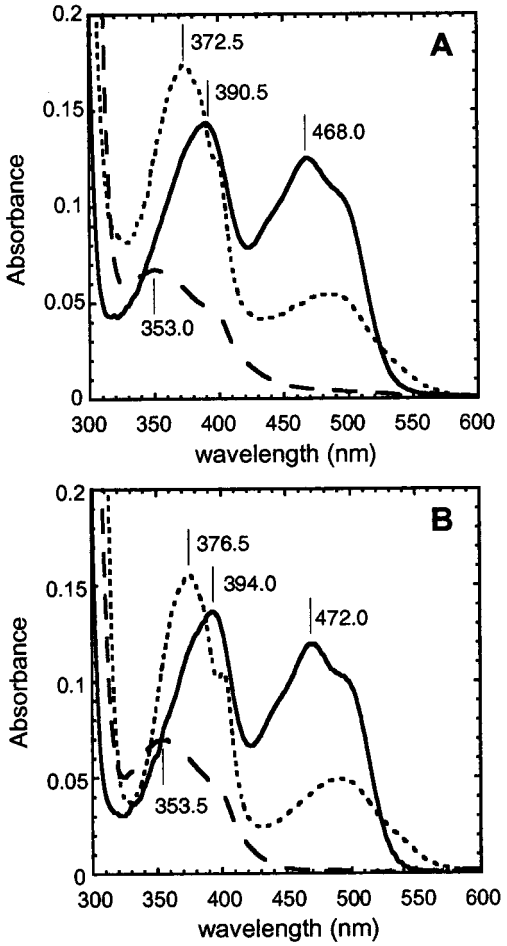

FIGURE 1: Visible spectra of (A) native and (B) N485L cholesterol oxidases for each oxidation state as determined by anaerobic reduction. (—) Oxidized, FAD; (- - -) semiquinone, FADH•; (— —) reduced, $FADH_2$. All spectra were acquired in 50 mM sodium phosphate buffer, pH 7.0. The semiquinone and reduced spectra were acquired under anaerobic conditions with benzyl viologen, xanthine, and xanthine oxidase as the reducing system, and the spectra of xanthine were subtracted for clarity. The semiquinone spectrum was determined by subtracting the small amount of oxidized species present near the midpoint of the titration and rescaled to 100%. The λ_{max} values of each species are indicated on the spectra.

Reduction Potential of FAD. The reduction potentials of the wild-type and N485L cofactors were measured spectroscopically using the dye-equilibration method of Massey (*16*). The 1 e^- reduction potentials of the N485L-oxidized FAD and semiquinone FAD are significantly reduced compared to wild type (Table 3). The midpoint potential is correspondingly reduced from −278 to −354 mV. The reduction potentials for cholesterol oxidase from *Streptomyces hygroscopicus* have been reported previously (*17*). The E_m of this enzyme is −217 mV, 60 mV higher than the cholesterol oxidase used in our work. Because there is no sequence or structural information available for the *Streptomyces hygroscopicus* enzyme, it is not possible to explain the difference between the two. It is clear, however, that bacteria produce multiple cholesterol oxidases with very different redox properties. For example, *Brevibacteria* produce one cholesterol oxidase that is structurally very similar to that used in this work (*6*, *22*), and a second that is structurally distinct with a covalently bound FAD (*23*) that has an increased redox potential (*17*, *24*).

Table 3: Reduction Potentials for Wild-Type and N485L Cholesterol Oxidases[a]

	max amount of semiquinone formed (%)	ΔE (mV)	E_1 (mV)	E_2 (mV)	E_m (mV)
wild type	98	−112	-222 ± 14	-334 ± 11	−278
N485L	95	−108	-300 ± 5	-408 ± 8	−354

[a] Determined spectroscopically using the xanthine and xanthine oxidase system (*16*) in 50 mM sodium phosphate, pH 7.0 at 15 °C. Safranin T was used as the redox standard ($E_m = -276$ mV).

Crystallographic Structure Analysis. As predicted from the CD spectra, the overall fold of N485L is identical to those of the native enzyme from *Streptomyces sp. SA-COO* (*6*) and *B. sterolicum* (*22*). Slight differences in the main chain atom positions between the mutant and native structures are localized at two loop regions (256−260 and 434−438). The electron density for the loop from residues 256−260 indicated a second conformation that was included in the final model. The loop from residues 434−438 forms part of the entrance to the active site cavity of the enzyme and has previously been observed to be poorly defined and highly mobile (*6*, *22*). In the mutant structure, the temperature factors for the main chain atoms in this loop region (28 $Å^2$) are significantly higher than the average observed for the entire protein (14 $Å^2$).

The substrate binding site of the native enzyme revealed 14 water molecules (*6*). All but one of these water molecules is retained in the active site of the N485L mutant. In the native structure, Wat1148 lies in a hydrophobic pocket, bounded by the side chains of Phe359, Trp351, Val124, and Ile379, and makes hydrogen bond contacts to both the side chain and the main chain atoms of Asn485 (Figure 2A). Due to the leucine mutation at this site, this water molecule is no longer present in the structure, and the residues surrounding this hydrophobic pocket are slightly repositioned to optimize van der Waals interactions (Figure 2B). The side chain of Met122 adopts a different conformation in the mutant structure ($\chi_3 = 85°$) compared to that of the native ($\chi_3 = -100°$) (Figure 3). Interestingly, the orientation of the methionine side chain is identical in the mutant and the dehydroisoandosterone complex structures (*10*). An ad-

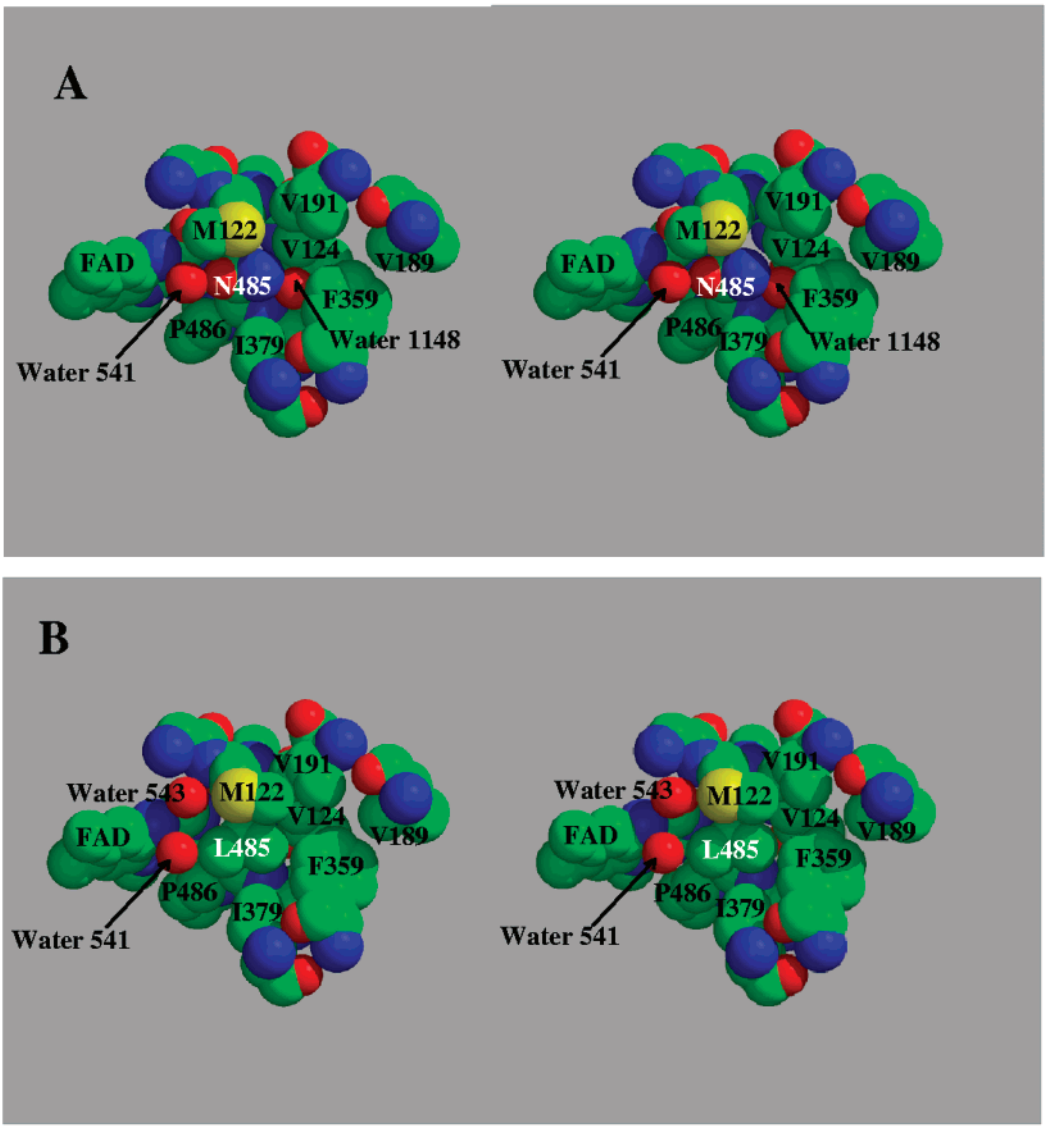

FIGURE 2: Stereo figure showing a CPK representation of the region around residue 485 in (A) the native enzyme structure and (B) the N485L mutant structure.

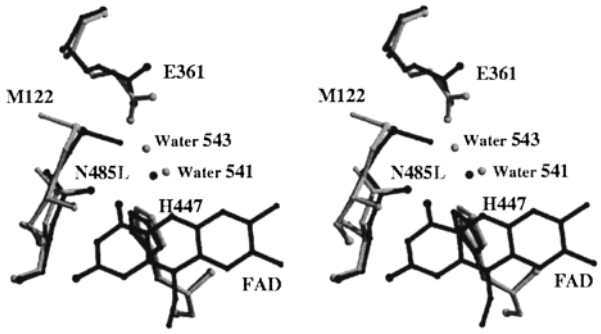

FIGURE 3: Stereo superposition of the active site residues for the native enzyme and the N485L mutant enzyme. The native structure is shown in black and the mutant in gray.

ditional water molecule (Wat543) is observed in the mutant structure in hydrogen bond contact to O4 of FAD. This water molecule lies near position of the Cϵ methyl group of Met122 in the native structures of both the *Streptomyces sp. SA-COO* and *B. sterolicum* enzymes. Furthermore, this water molecule lies in a similar position to the hydroxyl oxygen atom, O1′, of the dehydroisoandosterone steroid substrate in the complex structure.

Further changes in the active site of the mutant include a repositioning of Wat541 and His447. Both have been strongly implicated in substrate oxidation (*6*, *9*). In the native structure, Wat541 forms strong hydrogen bonds with the side chains of Asn485 and His447. In the mutant structure, the water molecule moves away from the side chain of Leu485, by 0.6 Å relative to the native water position (Figure 3). However, the hydrogen bond with His447 is still preserved due to a slight shift of the histidine side chain (0.3 Å).

Finally, changes in the active site of the mutant are observed for Glu361. In previously determined structures of the enzyme, this side chain exhibits high-temperature factors suggesting significant mobility. Furthermore, isotope labeling studies and site-directed mutagenesis of this residue have indicated it to be essential for the isomerization reaction of the enzyme (*6*, *25*−*27*). In the mutant structure, this glutamate side chain still has relatively high temperature factors (21.3 Å^2), and its α carbon position has shifted by 0.4 Å relative to the native enzyme. These observed structural changes in Glu361 place the carboxylate moiety within hydrogen bond distance to both the active site water molecule (541) and Wat543 (Figure 3).

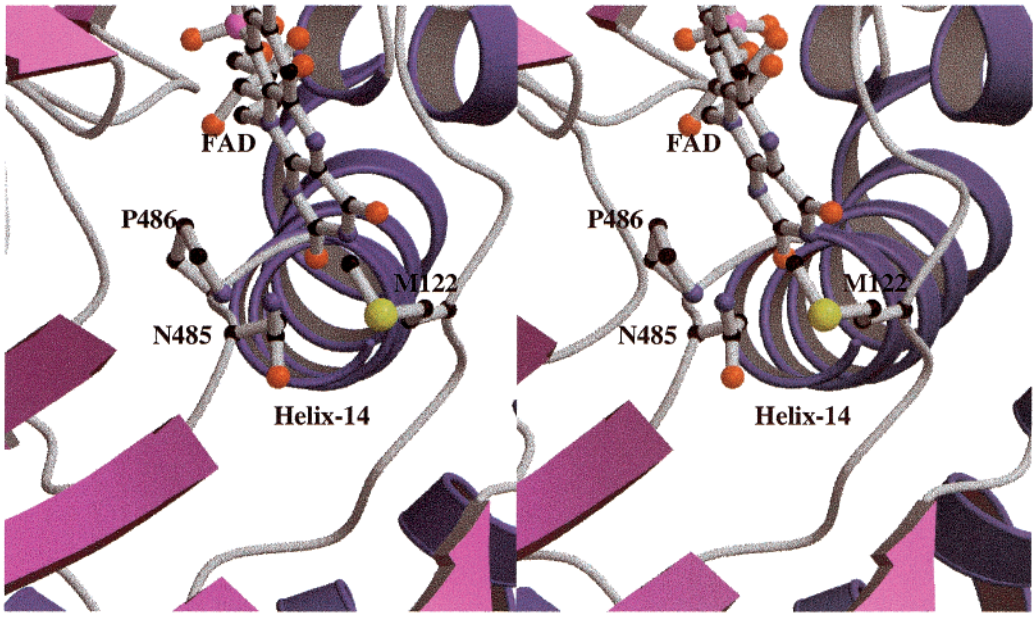

FIGURE 4: Stereoview of helix 14 in the native structure. The pyrimidine ring of the FAD cofactor and the side chains of Asn485, Pro486, and Met122 are shown located at the N-terminus of the helix.

DISCUSSION

The crystallographic models of *Streptomyces sp. SA-COO* and *B. sterolicum* cholesterol oxidase have revealed a structurally conserved active site. The positions of residues His447, Glu361, Asn485, and Wat541 suggest they play a role in the catalytic mechanism. [It should be noted that *B. sterolicum* has a second cholesterol oxidase that has a covalently bound FAD and is structurally distinct from the noncovalent form of the enzyme (*17, 23*).] Previously, we have shown that His447 via Wat541 is the general base for oxidation of the sterol (*6, 9*). Glu361 is the base that catalyzes the isomerization of cholest-5-en-3-one to cholest-4-en-3-one (*25*−*27*). Here, we investigated the importance of Asn485 in catalysis.

Asn485 plays a central role in forming the active site hydrogen-bonding network. It is positioned at the N-terminal end of helix 14; however, it is not involved in hydrogen bonding with the helix (Figure 4). The structures of the native enzyme from both *Streptomyces sp. SA-COO* and *B. sterolicum* show the Asn485 side chain oriented such that the amide nitrogen atom is within hydrogen-bonding distance of Wat541 (*10, 22*). However, the lack of a hydrogen-bonding network involving the amide nitrogen and oxygen atoms and discrete atoms on the protein makes unequivocal conformational assignment of the asparagine side chain impossible.

If the side chain nitrogen atom of Asn485 is hydrogen-bonded to Wat541, the helix dipole would increase hydrogen bond donation by Asn485, and increase the general acidity of Wat541. This orientation might lower the activation barrier to form the dienol intermediate of isomerization, but would simultaneously make the general-base-catalyzed oxidation more difficult. However, this side chain orientation would position the amide nitrogen atom within close contact with the isoalloxazine ring of FAD. This interaction would stabilize the electron-rich reduced form of the cofactor, thus promoting the oxidation reaction.

On the other hand, if the amide oxygen of Asn485 is hydrogen-bonded to Wat541, it would be poised to increase the general basicity of Wat541. However, the helix dipole would not favor reduction of negative charge on the amide oxygen. In addition, this orientation would position the electron-rich oxygen atom in close contact with the pyrimidine moiety of the isoalloxazine ring. This close interaction is unlikely and would decrease the reactivity of the FAD cofactor for oxidation.

Murooka and co-workers have reported that substitution of Asn485 with alanine and glutamine resulted in a lowering of oxidation activity, but not isomerization (*28*). However, they did not probe the reasons for these decreases in oxidation activity. To further test our proposition about the importance of Asn485, we designed and prepared an N485L mutant. Because leucine is isosteric with asparagine but is not polarizable or able to hydrogen bond, we expected to disturb the hydrogen-bonding network and disrupt the assistance from helix 14. Furthermore, this mutation would affect the electrostatic environment around the isoalloxazine ring and hence the reactivity of FAD. This mutation allowed us to assess Asn485's importance for maintaining the position of Wat541, for effecting general acid or base catalysis, and for altering the reduction potential of FAD.

Our kinetic results indicate that Asn485 plays a crucial role in the oxidation activity of the enzyme. When Asn485 was substituted with a leucine, the oxidation activity was greatly impaired. Steady-state kinetic analysis shows that k_{cat} for N485L is 1000-fold slower than wild type in oxidation and for isomerization is only 20-fold slower (Table 2). Increasing the pH of the wild-type enzyme decreases the oxidation activity 2000-fold and does not affect the isomerization activity. In contrast, for N485L, a 6-fold increase in oxidation activity was observed upon increasing pH. Although we cannot assign the pK_a to a single residue or site, the mutation of Asn485 to a more hydrophobic residue will change the electrostatic environment around the isoalloxazine ring system of the cofactor. These changes would affect the pK_a of the isoalloxazine N3 position which will alter the pH dependence of the oxidative activity of the enzyme. The

presence of a leucine in place of an asparagine near the cofactor likely results in an increased pK_a for the isoalloxazine N3. This altered electrostatic environment around the cofactor in the mutant enzyme may account for the retention of oxidative activity at high pH.

The slightly reduced isomerization rates upon mutation are probably due to a small shift in the position of the water structure in the active site. By analogy, the substrate position would be similarly shifted, and the substrate may no longer be ideally aligned with Glu361. Previously, we have observed that the position of Wat541 is important for maximal catalytic activity (*6*). This shift in position will also affect the alignment of the substrate with the FAD. However, the markedly lower oxidation activity of N485L implies that the major effect of the mutation is not primarily due to the misalignment of the substrate in the active site. Rather, it is the electrostatics of this residue that are most important for catalysis of oxidation.

Although the k_{cat}/K_m for the reaction is 1300-fold slower than wild type, 3α-H transfer is still rate-determining in the mutant reaction. This means that mutation of Asn485 reduces the rate of 3β-hydroxy oxidation, rather than decreasing the rate of another kinetic step. These primary isotope effects support the importance of Asn485 for FAD reduction. In contrast, when His447 is mutated, 3α-H transfer is no longer rate-determining (*9*). Mutation of His447 reduces the steady-state rate of oxidation at least 100-fold; however, either 3β-hydroxyl deprotonation (*9*) or $FADH_2$ oxidation becomes rate-determining (*29*).

We examined the X-ray crystal structure of the N485L mutant in order to determine the effect of the mutation on the active site structure. The most significant change observed in the mutant structure is a repositioning of Met122. In the native *B. sterolicum* and *Streptomyces* structures, the Cϵ of Met122 lies 3.3 and 3.0 Å, respectively, from O4 of FAD, suggestive of a C−H···O contact. In the mutant structure, the Cϵ of Met122 is repositioned due to the mutation to a leucine, forming a hydrophobic pocket made up of Val191, Leu485, Phe359, and Met122 (Figure 2). This altered side chain orientation recruits an additional water molecule (543) that forms a hydrogen bond with O4 of the FAD in the unliganded protein. Comparison of the structures of the N485L mutant with the dehydroisoandosterone complex reveals that, in the mutant, Wat543 is in a similar position to the hydroxyl oxygen of the steroid substrate in the complex. Interestingly, Met122 is in the hydrophobic pocket and does not contact O4 of the FAD. Moreover, the side chain Asn485 has rotated away from the pyrimidine ring of the cofactor (χ1 of Asn485 is −96° and −65° for the substrate-free and substrate-bound structures, respectively). Thus, the wild-type position of the methionine methyl group orients the amide group of Asn485 over the FAD. In addition, this close contact is observed in the native *B. sterolicum* structure as well as the E361Q and H447Q mutant structures from *Streptomyces* (*6*). In all of these structures, the position of Met122 is correlated with the position of residue 485.

The structural and kinetic data for N485L suggest that Asn485 and Met122 are important for creating an electrostatic potential around the FAD that is favorable for oxidation of alcohol substrates. Indeed, the UV/vis spectrum of the FAD region of N485L is red-shifted relative to wild type, indicating that the electronic environment around the FAD has been altered. In addition, the mutation of Asn485 to leucine and its associated structural changes result in a 76 mV decrease in the reduction potential of the FAD (Table 3). In other words, the N485L mutant is a much poorer oxidizing agent, and the reduction of the N485L-bound FAD is not as thermodynamically favorable as that of wild-type. This is consistent with the kinetic properties that we observe, i.e., a higher activation barrier to FAD reduction.

Thus, it appears that the most important role of Asn485 is to form an N−H···π electrostatic interaction to facilitate reduction of the FAD. Similar N−H···π interactions have been reported by Levitt and Perutz in studies of hemoglobin−drug interactions (*30*−*32*) and have been analyzed by Thornton (*33*−*35*). This is the first reported example of such an interaction between a protein residue and a flavin nucleus. Stabilization of the reduced flavin has been shown to involve interactions between protein atoms and discrete atoms on the isoalloxazine ring system of the cofactor, e.g., N1 and N5 (*36*−*40*). Rather than an atom−atom interaction between the protein and the cofactor, cholesterol oxidase reveals an atom−π interaction as providing the stabilization to the reduced form of the cofactor. Furthermore, the strength of this hydrogen bond is amplified by the presence of the dipole through helix 14 (Figure 4). This novel mechanism for flavin stabilization is supported by both structural and kinetic analysis. Empirical potential energy calculations have suggested that an N−H···π interaction has a stabilization energy of approximately 3 kcal/mol (*31*). This magnitude is consistent with a rate reduction of approximately 100-fold. The remainder of the 1300-fold rate reduction observed may be attributed to mispositioning of the substrate.

We conclude that the most important roles of Asn485 are 2-fold: first, to position Wat541, and consequently the substrate 3α-H, relative to the FAD and Glu361 to promote oxidation and isomerization; second, to create an electrostatic environment around the isoalloxazine ring that favors reduction of FAD by unactivated alcohols. The combination of kinetic, thermodynamic, and X-ray crystallographic data that we have acquired suggests that the polarity of the environment surrounding the isoalloxazine ring is as important for oxidation as a general base catalyst.

ACKNOWLEDGMENT

We thank Prof. Giovanni Gadda for his assistance with the redox potential measurements. We also thank Nathalie Croteau for crystallization of the mutant enzyme.

REFERENCES

1. Ohta, T., Fujishiro, K., Yamaguchi, K., Tamura, Y., Aisaka, K., Uwajima, T., and Hasegawa, M. (1991) *Gene 103*, 93−96.
2. Ishizaki, T., Hirayama, N., Shinkawa, H., Nimi, O., and Murooka, Y. (1989) *J. Bacteriol. 171*, 596−601.
3. Corbin, D. R., Greenplate, J. T., and Purcell, J. P. (1998) *HortScience 33*, 614−617.
4. Purcell, J. P., Greenplate, J. T., Jennings, M. G., Ryerse, J. S., Pershing, J. C., Sims, S. R., Prinsen, M. J., Corbin, D. R., Tran, M., Sammons, R. D., and Stonard, R. J. (1993) *Biochem. Biophys. Res. Commun. 196*, 1406−1413.
5. Corbin, D. R., Grebenok, R. J., Ohnmeiss, T. E., Greenplate, J. T., and Purcell, J. P. (2001) *Plant Physiol. 126*, 1116−1128.
6. Yue, K., Kass, I. J., Sampson, N., and Vrielink, A. (1999) *Biochemistry 38*, 4277−4286.
7. Cavener, D. R. (1992) *J. Mol. Biol. 223*, 811−814.

8. Kiess, M., Hecht, H. J., and Kalisz, H. M. (1998) *Eur. J. Biochem. 252*, 90−99.
9. Kass, I. J., and Sampson, N. S. (1998) *Biochemistry 37*, 17990−18000.
10. Li, J., Vrielink, A., Brick, P., and Blow, D. M. (1993) *Biochemistry 32*, 11507−11515.
11. Sampson, N. S., Kass, I. J., and Ghoshroy, K. B. (1998) *Biochemistry 37*, 5770−5778.
12. Nomura, N., Choi, K.-P., and Murooka, Y. (1995) *J. Ferment. Bioeng. 79*, 410−416.
13. Sambrook, J., Fritsch, E. F., and Maniatis, T. (1989) *Molecular Cloning: A Laboratory Manual*, 2nd ed., Cold Spring Harbor Laboratory Press, Cold Spring Harbor, NY.
14. Fasman, G. D. (1992) *Practical Handbook of Biochemistry and Molecular Biology*, CRC Press, Boca Raton, FL.
15. Smith, A. G., and Brooks, C. J. W. (1977) *Biochem. J. 167*, 121−129.
16. Massey, V. (1991) in *Flavins and Flavoproteins 1990* (Curti, B., Ronchi, S., and Zanetti, G., Eds.) pp 59−66, Walter de Gruyter & Co., Berlin, Germany.
17. Gadda, G., Wels, G., Pollegioni, L., Zucchelli, S., Ambrosius, D., M. S., P., and Ghisla, S. (1997) *Eur. J. Biochem. 250*, 369−376.
18. Otwinowski, Z. (1993) in *Data collection and Processing: Proceedings of the CCP4 Study Weekend* (Sawyer, L., Isaccs, N., and Bailey, S., Eds.) pp 56−62, SERC Daresbury Laboratory, Warrington, U.K.
19. Minor, W. (1993) *XDISPLAYF Program*, Purdue University.
20. Sheldrick, G. M., and Schneider, T. R. (1997) in *Methods in Enzymology* (Carter, C. W. J., and Sweet, R. M., Eds.) pp 319−343, Academic Press, Boston.
21. Bernstein, F. C., Koetzle, T. F., Williams, G. J., Meyer, E. E. J., Brice, M. D., Rodgers, J. R., Kennard, O., Shimanouchi, R., and Tasumi, M. (1977) *J. Mol. Biol. 112*, 535−542.
22. Vrielink, A., Lloyd, L. F., and Blow, D. M. (1991) *J. Mol. Biol. 219*, 533−554.
23. Coulombe, R., Yue, K. Q., Ghisla, S., and Vrielink, A. (2001) *J. Biol. Chem. 276*, 30435−30441.
24. Motteran, L., Pilone, M. S., Molla, G., Ghisla, S., and Pollegioni, L. (2001) *J. Biol. Chem. 276*, 18024−18030.
25. Kass, I. J., and Sampson, N. S. (1995) *Biochem. Biophys. Res. Commun. 206*, 688−693.
26. Kass, I. J., and Sampson, N. S. (1998) *Bioorg. Med. Chem. Lett. 8*, 2663−2668.
27. Sampson, N. S., and Kass, I. J. (1997) *J. Am. Chem. Soc. 119*, 855−862.
28. Yamashita, M., Toyama, M., Ono, H., Fujii, I., Hirayama, N., and Murooka, Y. (1998) *Protein Eng. 11*, 1075−1081.
29. Su, Q., and Klinman, J. P. (1999) *Biochemistry 38*, 8372−8381.
30. Levitt, M., and Perutz, M. F. (1988) *J. Mol. Biol. 201*, 751−754.
31. Perutz, M. F., Fermi, G., Abraham, D. J., Poyart, C., and Bursaux, E. (1986) *J. Am. Chem. Soc. 108*, 1064−1078.
32. Perutz, M. F. (1993) *Philos. Trans. R. Soc. London, Ser. A 345*, 105−112.
33. Singh, J., and Thornton, J. M. (1990) *J. Mol. Biol. 211*, 595−615.
34. Mitchell, J. B. O., Nandi, C. L., Ali, S., McDonald, I. K., Thornton, J. M., Price, S. L., and Singh, J. (1993) *Nature 366*, 413.
35. Mitchell, J. B. O., Nandi, C. L., MacDonald, I. K., Thornton, J. M., and Price, S. L. (1994) *J. Mol. Biol. 239*, 315−331.
36. Chang, F.-C., and Swenson, R. P. (1999) *Biochemistry 38*, 7168−7176.
37. Fraaije, M. W., and Mattevi, A. (2000) *Trends Biochem. Sci. 25*, 128−132.
38. Hoover, D. M., Drennan, C. L., Metzger, A. L., Osborne, C., Weber, C. H., Pattridge, K. A., and Ludwig, M. L. (1999) *J. Mol. Biol. 294*, 725−743.
39. Wagner, M. A., Trickey, P., Chen, Z.-W., Matthews, F. S., and Jorns, M. S. (2000) *Biochemistry 39*, 8813−8824.
40. van den Heuvel, R. H. H., Fraaije, M. W., Mattevi, A., and Van Berkel, W. J. H. (2000) *J. Biol. Chem. 275*, 14799−14808.

BI010843I